



ISSN: 0067-2904

Synthesis, Identification, Theoretical and Experimental Studies of Carbon Steel Corrosion Inhibition in Sea Water by Some New Diazine Derivatives linked to 5-Nitro Isatin Moiety

Athraa H. Ahmed*, Rehab M. Kubba, Suaad M. H. Al-Majidi

Department of Chemistry, College of Science, University of Baghdad, Baghdad, Iraq

Abstract

This research includes synthesis of new 5-Nitro isatin derivatives starting from 5-nitro-3-(imino acetohydrazide)-2-oxo indole (1) namely 5-nitro-3-[iminoaceto(tetra hydroypyridazin-3,6-dione)-2-yl]-2-oxo indole (2); 5-nitro-3-[iminoaceto(hexahydrodiazepine-3,7-dione)-2-yl]-2-oxo indole (3); 5-nitro-3-[iminoaceto (1,2-dihydro pyridiazin-3,6-dione)-2-yl]-2-oxo indole (4); 5-nitro-3-[iminoaceto (8-nitro- 1,2-dihydrophtalazin-3,10-dione)-2-yl]-2-oxo indole (5) and 5-nitro-3-[iminoaceto (1,2-dihydrophtalazin-3,10-dione)-2-yl]-2-oxo indole (6). The derivatives were characterized using FTIR, ¹HNMR, ¹³CNMR and C.H.N.S analysis with the measurement of some physical properties.

Quantum mechanical method of the Density Functional Theory (DFT) of B3LYP with a level of 6-311++G (2d, 2p) were used to calculate the geometrical structure, physical properties and inhibition efficiency parameters, were at the equilibrium geometry in four media (vacuum, DMSO, EtOH and H₂O). The theoretical results showed that compound (3) was the best corrosion inhibitor among the others. Finally, the corrosion inhibition, kinetics, and thermodynamics studies of the prepared compound (3) for carbon-steel in sea water had been conducted using the potentiodynamic polarization procedure, while the surface changes of the carbon steel were studied using SEM (Scanning Electron Microscopy) and AFM (Atomic Force Microscopy) techniques.

Keywords: 5-Nitro isatin, Diazine derivatives, Corrosion inhibitors, Quantum chemical calculations, Electrochemical measurements.

تحضير وتشخيص ودراسة نظرية وتجريبية لتثبيت تآكل حديد الصلب الكربوني في ماء البحر بفعل

بعض مشتقات الدايزين الجديدة المرتبطة مع 5- نايتر و ايساتين

عذراء حكمت أحمد*، رحاب ماجد كبة، سعاد محمد حسين الماجدي

كلية العلوم، قسم الكيمياء، جامعة بغداد، بغداد، العراق

الخلاصة

يتضمن البحث تحضير مشتقات جديدة من 5- نايتر و ايساتين بدأ من 5- نايتر و-3- (امينو اسيتو هايدرازيد)-2-اوكسو اندول (1) وهي 5- نايتر و-3- [امينو اسيتو(تيترا هيدروبايردازين-3,6-دايون)-2-يل]-2-اوكسو ادول (2); 5- نايتر و-3- [امينو اسيتو(هكسا هيدروبايردازين-3,7-دايون)-2-يل]-2-اوكسو ادول (3); 5- نايتر و-3- [امينو اسيتو(1,2-داي هيدروبايردازين-3,6-دايون)-2-يل]-2-اوكسو ادول (4); 5- نايتر و-3- [امينو اسيتو(8- نايتر و-1,2-داي هيدروفتالازين-3,10-دايون)-2-يل]-2-اوكسو ادول (5); 5- نايتر و-3- [امينو اسيتو(1,2-داي هيدروفتالازين-3,10-دايون)-2-يل]-2-اوكسو ادول (6).

*Email: hekmat@yahoo.com

يل-2-او كسو ادول (6). وتم تشخيص هذه المشتقات باستخدام مطيافية FTIR و $^1\text{H-NMR}$ و $^{13}\text{C-NMR}$ وتحليل عناصر C.H.N.S مع قياس بعض الخصائص الفيزيائية. وقد تم استخدام طريقة حسابات ميكانيك الكم وفق نظرية دوال الكثافة (DFT) عند المستوى-6 (B3LYP/311++G (2d,2p)) لحساب البنية الهندسية والخصائص الفيزيائية ومعاملات كفاءة التثبيط والتي تمت دراستها عند الشكل الهندسي المتوازن في أربعة أوساط (الفراغ والمذيبات DMSO و EtOH و H_2O). أظهرت نتائج الحسابات النظرية أفضلية المركب (3) كمثبط للتآكل من بين المشتقات الأخرى. وأخيراً، تمت دراسة كفاءة التثبيط ودراسة حركية وثرموديناميكية المركب (3) على حديد الصلب الكربوني في محلول 3.5% كلوريد الصوديوم باستخدام جهاز الاستقطاب المجهادي، وقياسات SEM (مجهر المسح الالكتروني) و AFM (مجهر القوة الذرية).

Introduction

Isatin is the reference compound of an important class of nitrogen-containing aromatic heterocyclic compounds, which have been found in many plants and tissue [1]. The pyridazine represents new pharmacologically active compounds. Diazines and their derivatives have become an important in chemistry. Diazines contain two azomethine nitrogen atoms. There are three types of diazines. The three diazines, pyridazine, pyrimidine and pyrazine are stable, colorless compounds, which are soluble in water [2].

Quantum chemical calculations had been used to study the reaction mechanism and to solve chemical ambiguities. This is a useful approach to investigate the reaction mechanism of the inhibitor molecule and the metal surface. The structural and electronic parameters of the inhibitor molecule can be obtained by theoretical calculations using the computational methodologies of quantum chemistry [3].

Corrosion inhibitors are chemicals that react with a metallic surface or the environments the metal surface is exposed to and act to protect the metal against corrosion [4]. Most organic compounds having hetero atoms (N, O, S) in their aromatic structure have been successfully used as corrosion inhibitors [5]. The heterogeneous organic compounds having higher basicity and electron density on the hetero atoms usually have tendency to resist corrosion.

The aim of the present work was to prepare new 5-nitro isatin derivatives, then studying theoretically their corrosion inhibition ability in four media (vacuum, DMSO, EtOH and water) for choosing the best corrosion inhibitor of them. This was done depending on parameters of quantum mechanical inhibition efficiency using DFT [6-311/ B3LYP++G (2d, 2p)] method. For proving that, the best corrosion inhibitor, expected theoretically (compound (3)) was studied experimentally as a corrosion inhibitor of carbon steel in sea water by the potentiodynamic polarization, SEM and AFM measurements technique.

Experimental part

Synthesis of 5-nitro-3-[iminoaceto(tetra hydroypyridazin-3,6-dione)-2-yl]-2-oxo indole (2), 5-nitro-3-[imino aceto(hexahydrodiazepine-3,7-dione)-2-yl]-2-oxo indole (3), 5-nitro-3-[iminoaceto (1,2-dihydro pyridiazin-3,6-dione)-2-yl]-2-oxo indole (4), 5-nitro-3-[iminoaceto (8-nitro- 1,2-dihydrophtalazin-3,10-dione)-2-yl]-2-oxo indole (5) and 5-nitro-3-[iminoaceto (1,2-dihydrophtalazin-3,10-dione)-2-yl]-2-oxo indole (6) [6].

To the mixture of hydrazid derivative (1) [7], (0.5 g, 0.0017 mol) with succinic anhydride, glutaric anhydride, maleic anhydride, 3-nitrophthalic anhydride or phthalic anhydride respectively (0.0017 mol) in 10 ml of glacial acetic acid, refluxed the mixture for (14) hours, then cooling by adding it on ice water. The obtained precipitate was filtered and recrystallized from ethanol solvent. The physical properties of compounds (2-6) are listed in Table-1.

Preparation of solutions

Blank solution

35 g of NaCl was dissolved in distilled water, then transferred to 1L volumetric flask, and 2 ml of DMSO was added, then the volume completed to 1 L with distal water.

5-Nitro-3-[imino aceto (hexahydrodiazepine-3,7-dione)-2-yl]-2-oxo indole (3) solutions

Three concentrations of (5, 10 and 20) ppm were prepared by dissolving (0.005, 0.01 and 0.02) g, of compound (3) respectively, in 2ml DMSO, transferred to a volumetric flask of 1L. Then 35g of NaCl

was added to each concentration after dissolving in distilled water before completing the volume to 1L.

Electrochemical measurements

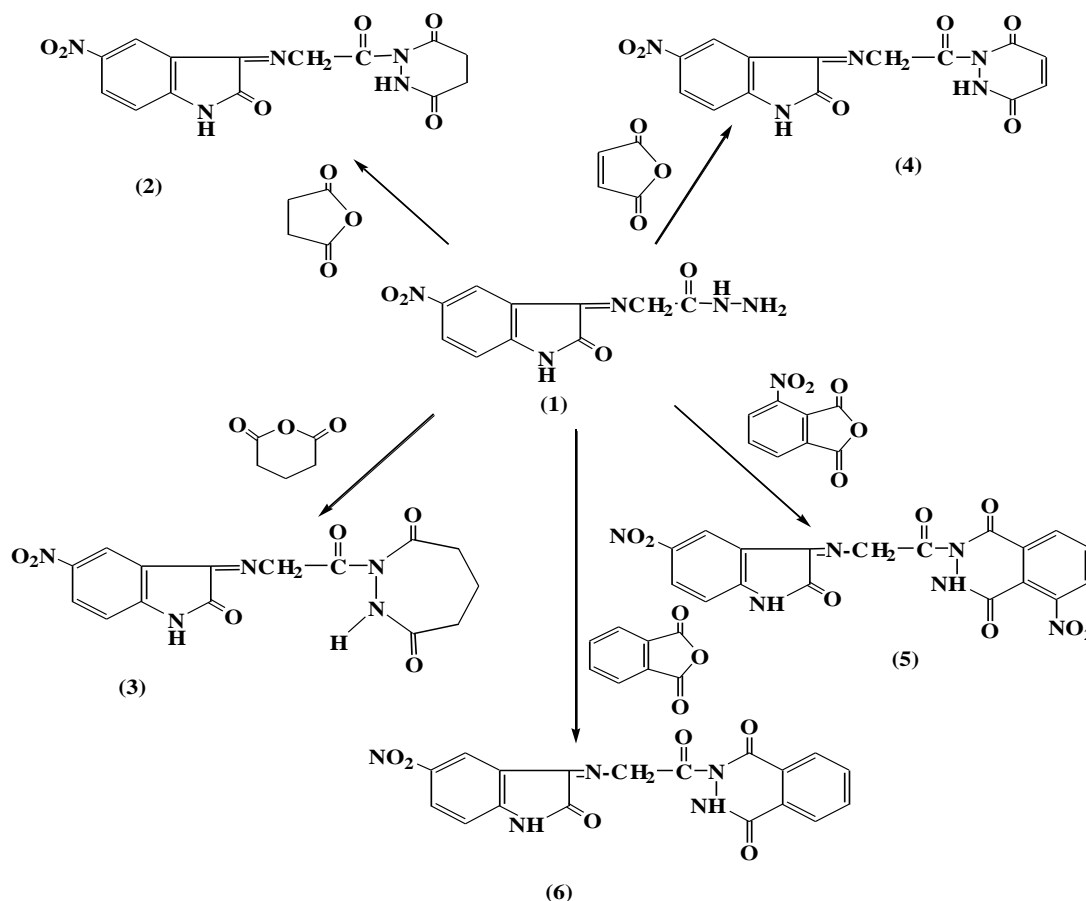
Potentiostatic polarization study

The potentiostat set up includes Host computer, thermostat, magnetic stirrer, Mat lab (Germany, 2000), potentiostat, and galvanostat. The corrosion cell is (1 L) capacity made of Pyrex consist of two bowls internal and external. The electrochemical corrosion cell is a three electrodes cell containing a working electrode carbon steel with 1cm^2 surface area used to determine the potential of working electrode according to the reference electrode, a platinum auxiliary electrode with length (10cm) and a silver-silver chloride (Ag/AgCl, 3.0M KCl) reference electrode. The working electrode was immersed in the test solution for 30 min. to establish state open circuit potential (E_{ocp}), then electrochemical measurements were performed in potential range of (± 200) mV. All tests were carried out at temperature of (298-318) K by controlling the cell temperature using a cooling heating circulating water bath.

Results and discussion

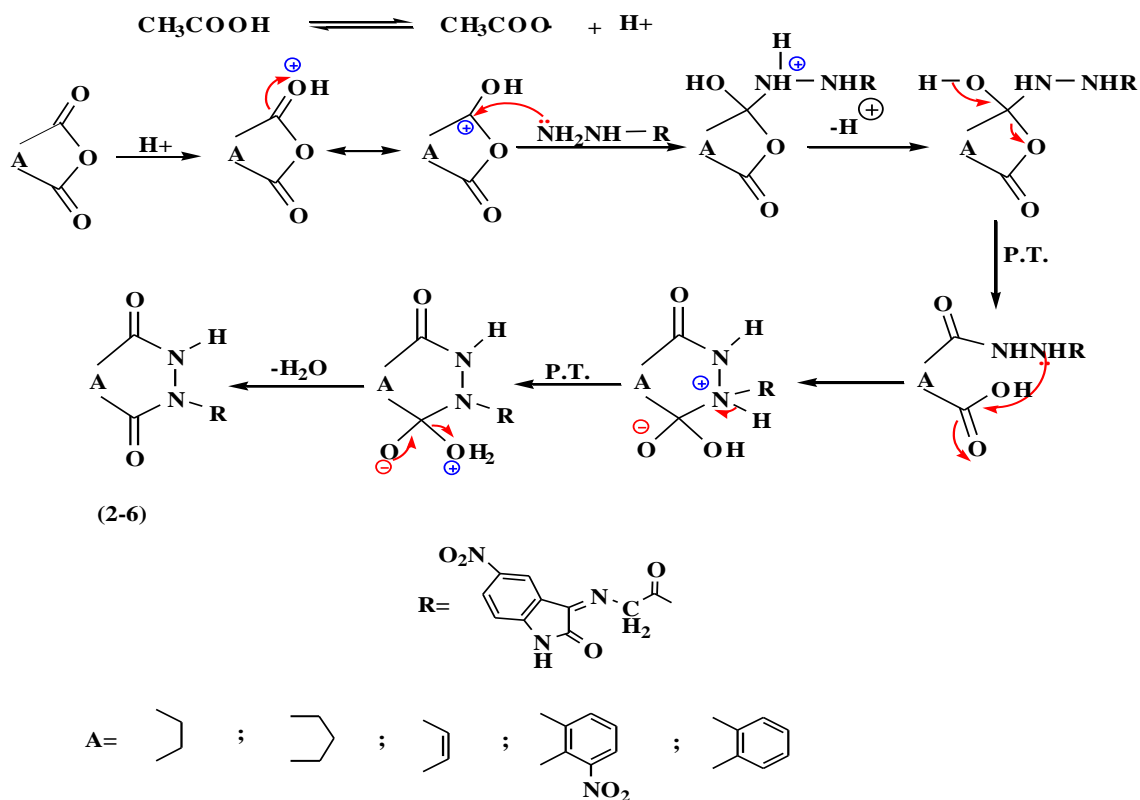
Synthesis of 5-Nitro isatin derivatives

Diazine compounds (**2-6**) were synthesized from the reaction of hydrazide derivative (**1**) with (succinic anhydride, glutaric anhydride, maleic anhydride, 4-nitrophthalic anhydride, and phthalic anhydride) respectively; in the presence of glacial acetic acid as a catalyst and as a solvent, Scheme 1.



Scheme 1

The mechanism for the synthesized derivatives is shown in Scheme 2 [7, 8].



Scheme 2

The FTIR spectra of compounds (2-6) show disappearance of two bands of (-NH₂) group of hydrazide derivative (1), and the appearance of a band due to (-NH) group at the range (3224-3245) cm⁻¹. Two carbonyl groups of compounds (2-6) appeared at (1721-1701) cm⁻¹ for cyclic carbonyl and at (1699-1688) cm⁻¹ for the amide carbonyl group, Table-2.

The ¹H-NMR spectrum for compound (3) was showed signal at δ=(3.72) ppm for (-CH₂-) protons, signal at δ= (4.23) ppm due to (O=C-CH₂) protons, singlet signal at δ= (4.99) ppm due to (=N-CH₂-) protons, multiple signal at δ= (7.04-8.27) ppm due to aromatic rings protons, singlet signal at δ= (8.29) ppm due to (N-N-H) proton and singlet signal at δ= (10.21) ppm due to (N-H indole ring) proton, Table-3.

The ¹H-NMR spectrum for compound (4) shown, singlet signal at δ= (3.62) ppm due to (=N-CH₂-) protons, triplet signal at δ= (6.21) ppm due to (-CH₂=CH₂-) protons, multiple signal at δ= (7.01-8.23) ppm due to aromatic rings protons, singlet signal at δ= (8.81) ppm due to (N-N-H) proton and singlet signal at δ= (10.19) ppm due to (N-H indole ring) proton, Table-3. The ¹³CNMR spectral data of compounds (3 and 4) are listed in Table-4. The C.H.N.S analysis for compound (3) is listed in Table-5.

Table 1-Physical properties of compounds (2-6)

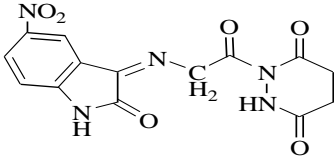
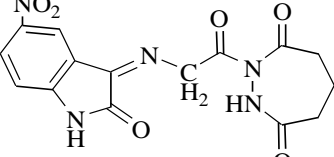
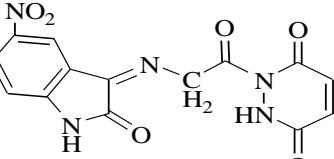
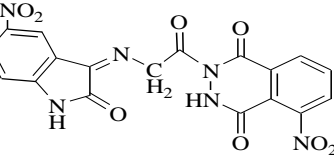
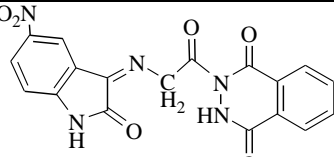
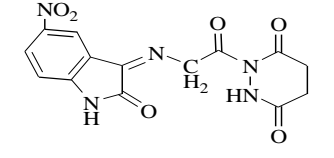
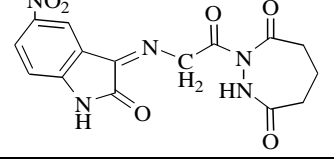
Com No.	Structure	Molecular formula	M.W g/mol	M.P °C	Yield %	Color	Solvent of Recryst.
2		C ₁₄ H ₁₁ N ₅ O ₆	345.27	183-185	80	Brown	Acetone
3		C ₁₅ H ₁₃ N ₅ O ₆	359.29	168-169	70	Brown	Chloro form
4		C ₁₄ H ₉ N ₅ O ₆	343.25	183-184	73	Brown	Dichloro-methan
5		C ₁₈ H ₁₀ N ₆ O ₈	438.31	237-239	88	Pale orange	Chloro form
6		C ₁₈ H ₁₁ N ₅ O ₆	393.31	237-239	65	Pale orange	Chloro form

Table 2- FTIR spectral data (ν , cm⁻¹) of compounds (2-6)

Com . No.	Structure	FTIR spectral data cm ⁻¹					
		ν (N-H)	ν (C-H) arom.	ν (C-H) aliph.	ν (C=O) Amide	ν (C=N)	Others
2		3226	3076	2921 2852	1710 1688	1623	ν (NO ₂) Asym. 1519 Sym. 1338
3		3245	3088	2921 2852	1711 1692	1622	ν (NO ₂) Asym. 1521 Sym. 1338

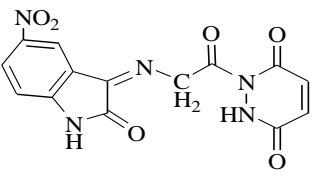
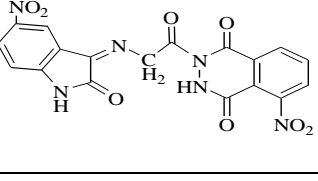
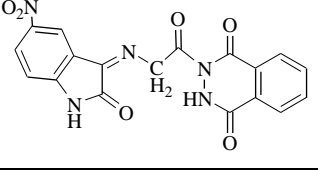
4		3226	3082	2921 2852	1701 1688	1623	v(NO ₂) Asym. 1519 Sym. 1340 (=CH ₂) 1598
5		3226	3075	2921 2850	1713 1699	1622	v(NO ₂) Asym. 1542 Sym. 1336
6		3224	3082	2923 2850	1721 1699	1625	v(NO ₂) Asym. 1519 Sym. 1340

Table 3- ¹H-NMR spectral data (δ, ppm) for compounds (3 and 4)

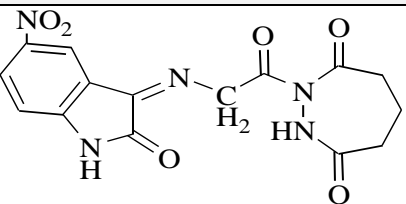
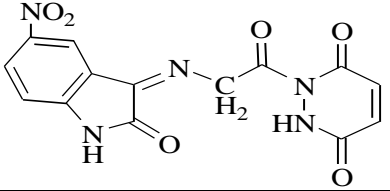
Com. No.	Structure	¹ HNMR Spectral data (δ, ppm)
3		3.72 (m, 2H, -CH ₂ -); 4.23 (t, 4H, O=C-CH ₂ -); 4.99 (s, 2H, =N-CH ₂ -); 7.04-8.27 (m, 3H, Ar-H); 8.29 (s, 1H, N-N-H); 10.21 (s, 1H, N-H indole ring).
4		3.62 (s, 2H, =N-CH ₂ -); 6.21 (t, 4H, -CH ₂ =CH ₂); 7.01-8.23 (m, 3H, Ar-H); 8.81 (s, 1H, N-N-H); 10.19 (s, 1H, N-H indole ring).

Table 4- ¹³C-NMR spectral data (δ, ppm) for compounds (3 and 4)

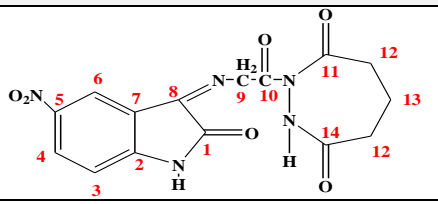
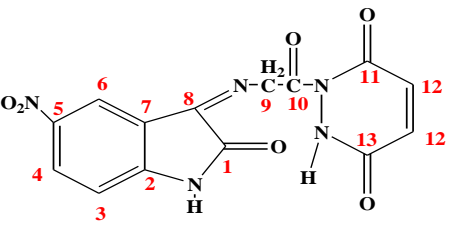
Com. No.	Structure	¹³ CNMR Spectral data (δ, ppm)
3		20 (C13); 36 (C12); 73 (C9); 111-138 (C2, 3, 4, 5, 6, 7); 146 (C8); 162 (C1); 165 (C10); 168 (C11, 14).
4		76 (C9); 111-123 (C2, 3, 4, 5, 6, 7); 136 (C12) 143 (C8); 160 (C1); 163 (C10); 170 (C11, 13).

Table 5-The C.H.N.S analysis for compound (3)

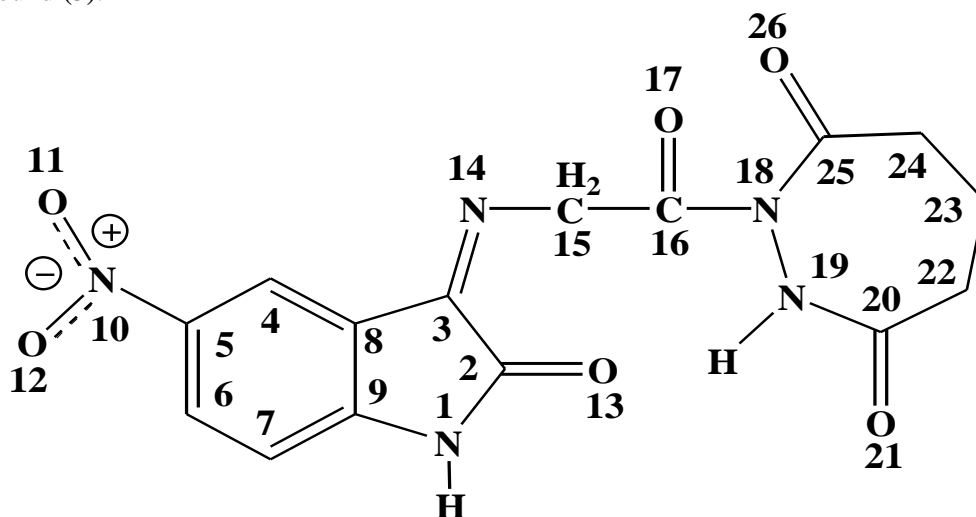
Com. No.	Molecular Formula	Calculated, (%)				Found, (%)			
		C	H	N	S	C	H	N	S
3	C ₁₆ H ₁₄ N ₄ O ₆	53.63	3.94	15.64	---	53.50	3.90	15.55	---

Quantum chemical calculations

The structural nature of the organic inhibitors and their inhibition mechanism were described by density functional theory (DFT). The inhibition efficiencies of compounds (2-6) were investigated by the theoretical corrosion inhibition parameters such as energy of the highest occupied molecular orbital (E_{HOMO}) and energy of the lowest unoccupied molecular orbital (E_{LUMO}), energy gap (ΔE) between E_{HOMO} and E_{LUMO} , dipole moment (μ), electronegativity (χ), electron affinity (A), global hardness (η), softness (σ), ionization energy (IE), global electrophilicity (ω), the fraction of electrons transferred (ΔN) and the total energy (E_{tot}) [9].

Molecular geometry

The compounds were built using Chem Draw of Mopac program. Gaussian 09 package was used for calculating the equilibrium geometry [10]. The corresponding geometry in the vacuum phase was fully optimized using DFT (Density Functional Theory) which was carried out using basis set of (B3LYP) with a 6-311++G (2d, 2p) level of theory [11,12]. Also the equilibrium geometry was calculated in three solvent media (EtOH, DMSO and H₂O). Figure-1 shows the numbering of atoms of compound (3).

**Figure 1-**The numbering of atoms for compound (3).

The computational structural parameters such as bond angles, bond distances and dihedral angles were studied. The longest bond length was observed for C22-C23 (1.539Å). The shortest bond length was observed for N19-H (1.017Å). The bond angles were getting between (105.242Å) for H2C15C16 and (131.308Å) for C3C8C4. The values of the dihedral angles (trans & cis) were proved that the compound was not planar [the cis dihedral angles are not of 0.0 degree and all of the trans dihedral angles are more or less than 180.0 degree], Table-6.

Table 6-Geometrical structure for compound (3) in the media of (vacuum, EtOH, DMSO, and H₂O) as calculated by using DFT method

Description Bond length	Bond length (Å)	Description angle (deg)	Angle (deg)	Description Dihedral angle(deg)	Dihedral angle (deg)
C3-C8	1.466	C4C5N10	118.979	N1C2C3C8	-3.681
C3-N14	1.265	C6C5N10	118.743	N1C2C3N14	177.481

C4-C5	1.390	C5C6C7	120.292	HN1C2O13	-19.347
C4-C8	1.380	C6C7C9	117.731	C2C3C8C4	-178.594
C5-C6	1.391	C3C8C9	107.856	C2C3C8C9	0.703
C5-N10	1.472	C3C8C4	131.308	C3C8C9C7	-179.265
C6-C7	1.391	C7C9N1	128.583	C3C8C9N1	2.586
C7-C9	1.385	C8C9N1	109.823	C8C4C5C6	-0.047
C8-C9	1.402	C5N10O11	117.839	C8C4C5N10	-179.946
N10-O11	1.224	C5N10O12	117.987	C4C5C6C7	0.401
N10-O12	1.226	C3N14C15	121.621	N10C5C6C7	-179.698
N14-C15	1.452	N14C15C16	109.216	C2C3N14C15	-0.258
C15-H2	1.091	N14C15H2	108.191	C3N14C15C16	158.824
C15-C16	1.523	H2C15C16	105.242	N14C15C16O17	71.532
C16=O17	1.209	C15C16O17	123.108	N14C15C16N18	-112.403
C16-N18	1.392	O17C16N18	120.826	C15C16N18N19	176.239
N17-N19	1.419	C16N18N19	113.851	C16N17N19C20	121.777
N19-H	1.017	N18N19H	109.229	O17C16N18N19	-7.599
N19-C20	1.395	N18N19C20	120.346	C16N18N19H	-11.503
C20=O21	1.209	N19C20O21	120.017	N18N19C20O21	153.537
C20-C22	1.510	N19C20C22	115.697	N18N19C20C22	32.185
C22-C23	1.539	C20C22C23	114.022	N19C20C22C23	44.730
C23-C24	1.538	C22C23C24	115.057	C20C22C23C24	-81.674
C24-C25	1.505	C23C24C25	115.780	C22C23C24C25	63.548
C25=O26	1.197	C24C25O26	124.880	C23C24C25O26	132.794

Global molecular reactivity:

Frontier orbital theory is used in predicting adsorption centers of the inhibitor responsible of the reaction metal surface/ molecule [13]. The calculated quantum chemical parameters related to the inhibition efficiency of the studied molecule are collected in Tables- (7a, 7b). They are calculated according to the following equations:

$$\text{IP (Ionization potential)} = -E_{\text{HOMO}} \quad (1)$$

$$\text{EA (Electron affinity)} = -E_{\text{LUMO}} \quad (2)$$

$$\text{H (Hardness)} = (\text{IE} - \text{EA}) / 2 \quad (3)$$

$$\text{X (Electro negativity)} = (\text{IE} + \text{EA}) / 2 \quad (4)$$

The Global softness (S) is the inverse of the global hardness.

$$\text{S (global softness)} = 1 / \eta \quad (5)$$

The Global electrophilicity index (ω) introduced by Parr [14], using for calculating the electronegativity and chemical hardness parameters, Equation 6:

$$\text{Global electro philicity index } (\omega) = (-\chi)^2 / 2\eta = \mu^2 / 2\eta \quad (6)$$

The fraction of electrons transferred (ΔN) from an inhibitor to carbon steel surface was also calculated using theoretical χ_{Fe} and η_{Fe} values for mild steel of 7.0 eV mol⁻¹ and 0.0 eV mol⁻¹, respectively. The number of transferred electrons (ΔN) was also calculated [15] by using the Equation (7).

$$\Delta N (\text{Electron transferred}) = (\chi_{\text{Fe}} - \chi_{\text{inhib.}}) / [2 (\eta_{\text{Fe}} + \eta_{\text{inhib.}})] \quad (7)$$

The calculated quantum chemical parameters in the vacuum, EtOH, DMSO and H₂O had shown a good effect for increasing the efficiency inhibition for compound (3), Tables-(7a, 7b).

Figure-2 showed the geometry optimization of compound (3) in the vacuum including HOMO and LUMO density distributions. The HOMO mainly located on the diazine moiety, this would indicate that the preferred active sites for an electrophilic attack are located within the region around the nitrogen atoms. Moreover, the electronic density of LUMO was distributed at the aromatic ring and around the ring of isatin moiety (which is the most planar region in the molecule), Figure-2.

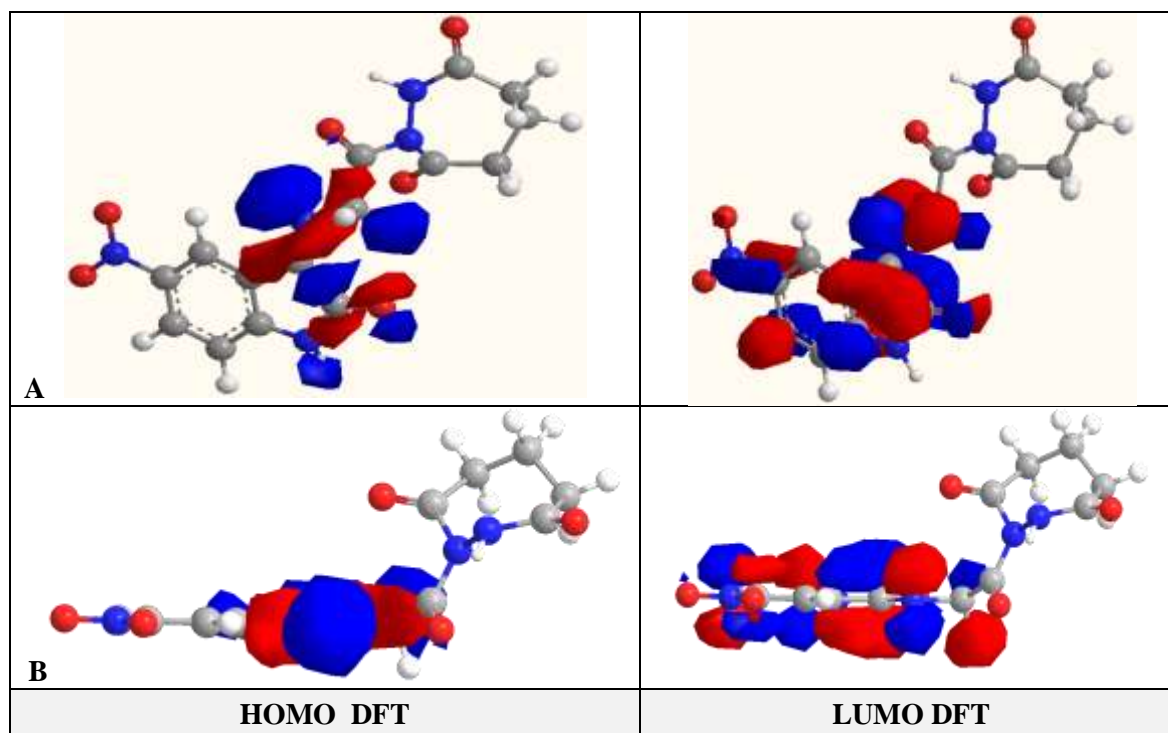


Figure 2-A) The Frontier Molecular Orbital density distributions of the studying 5-Nitro isatin derivative using. B- The most planar region in the molecule. [Red color: negatively charged lobe; blue color: positive charge lobe].

Table 7a-DFT calculations for some physical properties of the inhibitor molecules (2-6) at the equilibrium geometry

Inhib. media	P. G.	M. formula	E _{HOMO} (eV)	E _{LUMO} (eV)	ΔE _{HOMO-LUMO} (eV)	μ (Debye)	E _{total} (eV)
(2)							
Vacuum	C1	C ₁₄ H ₁₁ N ₅ O ₆	-7.177	-3.344	3.832	7.642	-34435.6
EtOH	C1		-7.093	-3.184	3.909	10.311	-34436.5
DMSO	C1		-7.088	-3.181	3.907	10.420	-34436.5
H ₂ O	C1		-7.086	-3.180	3.905	10.472	-34436.5
(3)							
Vacuum	C1	C ₁₅ H ₁₃ N ₅ O ₆	-7.144	-3.302	3.841	9.735	-35506.0
EtOH	C1		-7.102	-3.112	3.989	13.183	-35506.8
DMSO	C1		-7.095	-3.110	3.985	13.324	-35506.8
H ₂ O	C1		-7.092	-3.109	3.983	13.390	-35506.8
(4)							
Vacuum	C1	C ₁₄ H ₉ N ₅ O ₆	-7.378	-3.578	3.800	7.145	-34402.7
EtOH	C1		-7.154	-3.404	3.750	9.624	-34402.7
DMSO	C1		-7.146	-3.402	3.743	9.713	-34403.5
H ₂ O	C1		-7.142	-3.401	3.740	9.755	-34403.5

(5)							
Vacuum	C1	C ₁₈ H ₁₀ N ₆ O ₈	-7.406	-3.470	3.936	8.157	-44150.9
EtOH	C1		-7.126	-3.176	3.950	10.946	-44151.8
DMSO	C1		-7.117	-3.170	3.947	11.060	-44151.9
H ₂ O	C1		-7.113	-3.167	3.945	11.114	-44151.9
(6)							
Vacuum	C1	C ₁₈ H ₁₀ N ₅ O ₆	-7.172	-3.292	3.879	8.341	-38585.0
EtOH	C1		-7.092	-3.158	3.933	11.216	-38585.7
DMSO	C1		-7.087	-3.157	3.930	11.330	-38585.7
H ₂ O	C1		-7.085	-3.156	3.928	11.383	-38585.8

Table 7b-Quantum chemical parameters for inhibitor molecules (2-6) as calculated by using DFT method

Inhib. Media	IE (eV)	EA (eV)	□ (eV)	□ (eV)	S (eV)	ω (eV)	ΔN
(2)							
Vacuum	7.177	3.344	1.916	5.261	0.521	7.221	0.4536
EtOH	7.093	3.184	1.954	5.138	0.511	6.754	0.4761
DMSO	7.088	3.181	1.953	5.135	0.511	6.748	0.4773
H ₂ O	7.086	3.180	1.952	5.133	0.512	6.746	0.4779
(3)							
Vacuum	7.144	3.302	1.921	5.223	0.520	7.102	0.4622
EtOH	7.102	3.112	1.994	5.107	0.501	6.539	0.4742
DMSO	7.095	3.110	1.992	5.102	0.501	6.533	0.4760
H ₂ O	7.092	3.109	1.991	5.100	0.502	6.531	0.4767
(4)							
Vacuum	7.378	3.578	1.900	5.478	0.526	7.897	0.4004
EtOH	7.154	3.404	1.875	5.279	0.533	7.432	0.4586
DMSO	7.146	3.402	1.871	5.274	0.534	7.431	0.4609
H ₂ O	7.142	3.401	1.870	5.272	0.534	7.431	0.4620
(5)							
Vacuum	7.406	3.470	1.968	5.438	0.508	7.513	0.3968
EtOH	7.126	3.176	1.975	5.151	0.506	6.717	0.4680
DMSO	7.117	3.170	1.973	5.143	0.506	6.703	0.4703
H ₂ O	7.113	3.167	1.972	5.140	0.506	6.695	0.4713
(6)							
Vacuum	7.172	3.292	1.939	5.232	0.515	7.057	0.4556
EtOH	7.092	3.158	1.967	5.125	0.508	6.678	0.4763
DMSO	7.087	3.157	1.965	5.122	0.508	6.676	0.4777
H ₂ O	7.085	3.156	1.964	5.120	0.509	6.674	0.4783

Active sites of the compound (3)

The inhibition of the investigated inhibitor was done through its reactive centers (nucleophilic and electrophilic centers) using the DFT Mulliken charges population analysis. Table-8 shows that the oxygen, nitrogen and some carbon atoms have the higher negative charge, whereas C2, C3, C8 and C20 atoms have the higher positive electron density. Destinations for nucleophilic reactive sites of compound (3) were be O13, O17, N19, O21, O26 and the carbon atoms which have negative charge could be considered to be as an active adsorption center towards the metal surface.

The nucleophilic and electrophilic electronic charge values of compound (3) are stronger in EtOH, DMSO and H₂O solutions than in vacuum.

Table-8 shows that the order of the nucleophilic reactive sites are N19 < O26 < C7 < O13 < O17 < O21 < C4, and the electrophilic reactive sites order are C3 < C2 < C20 < C8.

Table 8-DFT Mulliken charges population analysis for the calculated inhibitor molecule compound (3) in media (vacuum, EtOH, DMSO, and H₂O).

Atom	Electronic charge (ecu)	Atom	Electronic charge (ecu)	Atom	Electronic charge (ecu)	Atom	Electronic charge (ecu)
N1	-0.221V	C8	0.791V	C15	0.039V	C22	-0.122V
	-0.213E		0.808E		0.054E		-0.146E
	-0.212D		0.809D		0.055D		-0.147D
	-0.212W		0.809W		0.056W		-0.148W
C2	0.276V	C9	-0.409V	C16	0.155V	C23	-0.037V
	0.343E		-0.460E		0.188E		-0.029E
	0.346D		-0.462D		0.189D		-0.028D
	0.347W		-0.463W		0.190W		-0.028W
C3	0.310V	N10	0.025V	O17	-0.429V	C24	0.005V
	0.351E		0.079E		-0.496E		0.000E
	0.353D		0.081D		-0.499D		0.000D
	0.354W		0.082W		-0.500W		0.000W
C4	-0.641V	O11	-0.130V	N18	0.016V	C25	-0.111V
	-0.612E		-0.191E		0.056E		-0.087E
	-0.611D		-0.193D		0.058D		-0.087D
	-0.611W		-0.194W		0.059W		-0.086W
C5	0.106V	O12	-0.158V	N19	-0.237V	O26	-0.346V
	0.058E		-0.208E		-0.246E		-0.391E
	0.056D		-0.210D		-0.246D		-0.393D
	0.055W		-0.210W		-0.246W		-0.393W
C6	0.158V	O13	-0.442V	C20	0.332V	-----	-----
	0.185E		-0.489E		0.393E		-----
	0.186D		-0.490D		0.395D		-----
	0.186W		-0.490W		0.396W		-----
C7	-0.442V	N14	-0.079V	O21	-0.434V	-----	-----
	-0.466E		-0.146E		-0.517E		-----
	-0.467D		-0.150D		-0.520D		-----
	-0.467W		-0.151W		-0.521W		-----

V: vacuum phase, D: dimethyl sulfoxide (DMSO), W: water, ecu: electron control unit.

Corrosion inhibition measurement

Potentiodynamic polarization curves and corrosion kinetic

The electrochemical corrosion parameters are presented in Table 9 such as corrosion potential (E_{corr}), Tafel slopes (bc, ba) and corrosion current density (I_{corr}) obtained by of cathodic and anodic regions of the Tafel lines. Figure-3 presents potentiodynamic polarization curves for C.S in sea water containing different conditions of compound (3). IE%, Θ , can be measured using the following Equations:

$$\% \text{IE} = (I_{\text{corr (uninh)}} - I_{\text{corr (inh)}}) / I_{\text{corr (uninh)}} \times 100 \quad (8)$$

$$\Theta = (I_{\text{corr (uninh)}} - I_{\text{corr (inh)}}) / I_{\text{corr (uninh)}} \quad (9)$$

Where $I_{\text{corr (inh)}}$ is the inhibited corrosion current densities, $I_{\text{corr (uninh)}}$ is the uninhibited current densities.

Table-9 shown the decreasing in IE% with the increasing temperature which may be indicating a physisorption inhibition process [16].

Table 9-Electrochemical data of the C.S corrosion in sea water at different concentrations for compound (3).

Inhibitor Conc. (mg/L)	T/ K	E _{corr} (mV)	I _{corr} (μA cm ⁻²)	b _c (mV dec ⁻¹)	b _a (mV dec ⁻¹)	IE%	Θ
Blank	298	-621.0	121.69	-146.9	82.1	-	---
	308	-785.7	164.53	-26.3	73.8	-	---
	318	-608.0	191.16	-102.0	315.2	-	---
5	298	-537.3	27.44	-377	102.7	77.451	0.775
	308	-530.0	41.84	-434.4	106.8	74.570	0.746
	318	-622.9	55.16	-138.8	61.4	71.145	0.711
10	298	-562.9	24.6	-231.5	79.6	79.784	0.797
	308	-491.3	36.09	-426.4	91.6	78.064	0.780
	318	-631.9	45.52	-106.9	59.5	76.187	0.761
20	298	-483.1	20.48	-358.3	55.9	83.170	0.831
	308	-498.1	32.53	-115.4	68.5	80.228	0.802
	318	-598.0	42.01	-222.6	92.3	78.023	0.780

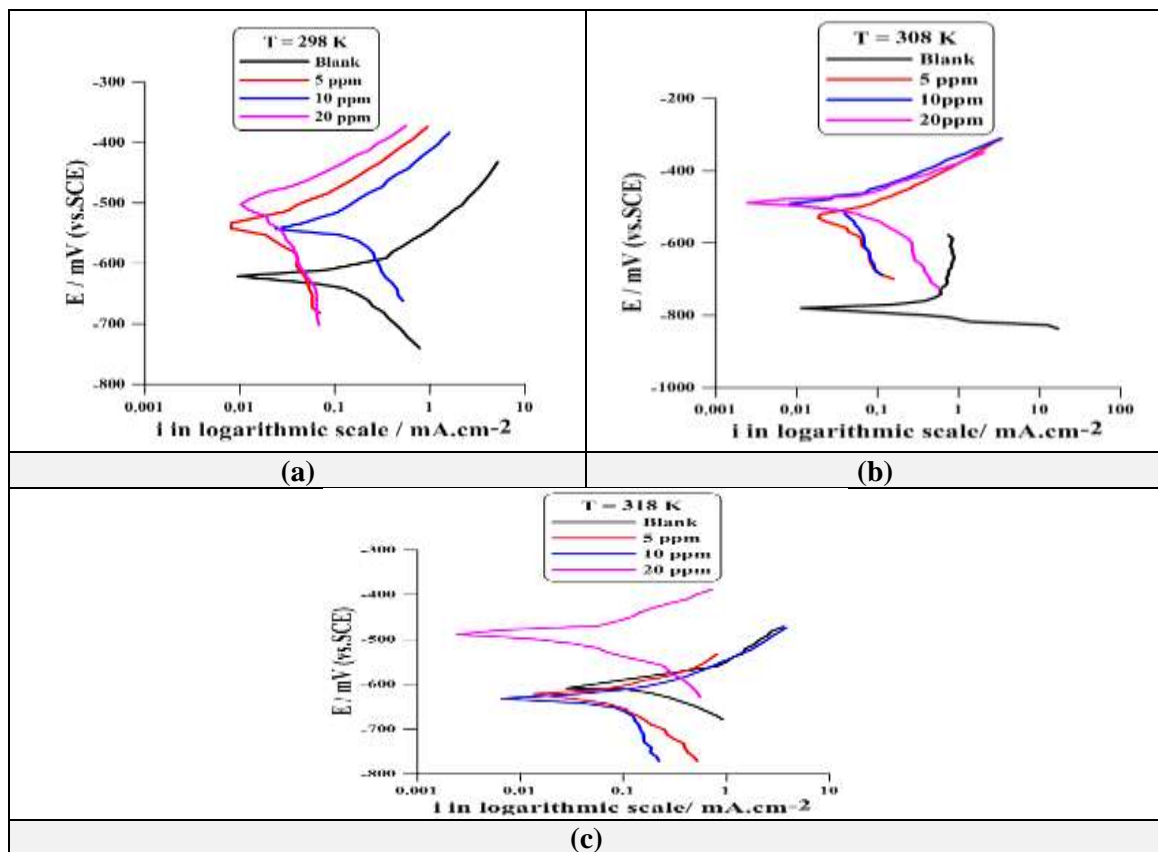


Figure 3-Polarisation curve of C.S in sea water for different concentrations of compound (3) at temperature (a) 293K (b) 308K (c) 318 K.

Thermodynamic and activation parameters

The Arrhenius law presented as a straight line of the logarithm of the corrosion rate. The straight line plots between $\log I_{\text{corr}}$ and $1/T$ are shown in Figure-4. The activation energy of the corrosion process (E_a), and the pre-exponential factor (A), are calculating from Equations 11 and 12.

$$\text{Log } (I_{\text{corr}}) = \text{Log } A - E_a / 2.303RT \quad (11)$$

$$\text{Log } (I_{\text{corr}}/ T) = \text{Log } (R/ N h) + \Delta S^*/ 2.303R - \Delta H^*/ 2.303RT \quad (12)$$

Where (I_{corr}) is the corrosion current density, (R) is the universal gas constant ($8.314 \text{ J} \cdot \text{mol}^{-1} \cdot \text{K}^{-1}$), (T) is temperature in K, (h) is the Plank's constant ($6.626 \times 10^{-34} \text{ J s}$), (N) is the Avogadro's number ($6.022 \times 10^{23} \text{ mol}^{-1}$), ΔH is the enthalpy of activation and ΔS is the entropy of activation.

A plot of $\log (I_{\text{corr}}/ T)$ against $(1/T)$ gave linear relationship with a slope of $(-\Delta H^*/ 2.303R)$ and an intercept of $[\log(R/ N h) + (\Delta S^*/ 2.303R)]$ as shown in Figure-5, from which the activation thermodynamic parameters (ΔH^* and ΔS^*) were calculated, Table-10.

The enthalpy changes (ΔH^*) of the corrosion reaction in 3.5% NaCl at temperature range of (298-318) K have positive values indicating an endothermic nature for this reaction [17]. The lower negative values of entropy (ΔS^*) for corrosion process meaning a decrease in the degree of freedom and a consequent restriction of the corrosion process [18]

The values of ΔG for corrosion process were calculated from the following relation:

$$\Delta G^* = \Delta H^* - T \Delta S^* \quad (13)$$

Table 10-Corrosion kinetic parameters for carbon steel in sea water (3.5% NaCl) for blank and with various concentrations of the inhibitor.

Conc. (mg/ L)	$\Delta G/ \text{kJ mol}^{-1}$			$\Delta H^*/ \text{kJ. mol}^{-1}$	$\Delta S^*/ \text{kJ. mol}^{-1} \cdot \text{K}^{-1}$	$E_a / \text{kJ} \cdot \text{mol}^{-1}$	A Molecules. $\text{cm}^{-2} \text{S}^{-1}$
	298K	308K	318K				
Blank	61.037	62.572	64.107	15.29 3	-0.154	17.853	1.006E+29
5	65.469	66.927	68.385	22.01 9	-0.146	27.553	2.53861E+29
10	65.722	67.143	68.564	23.37 9	-0.142	24.298	3.97737E+29
20	66.107	67.498	68.890	24.64 2	-0.139	28.376	5.65713E+29

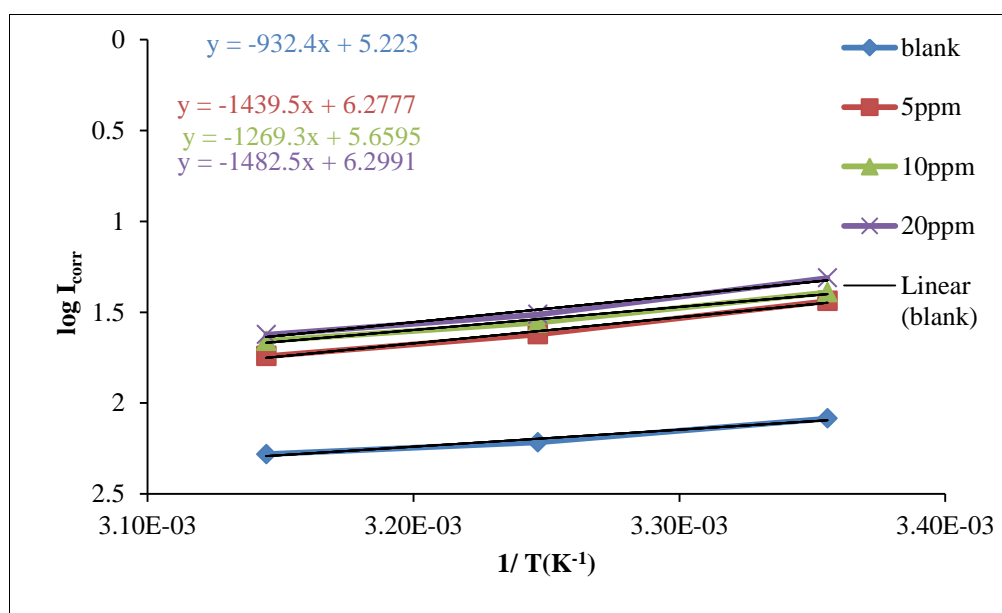


Figure 4-Plot of $\log I_{\text{corr}}$ vs $(1/T)$ for the corrosion for carbon steel in sea water (3.5% NaCl) containing different concentrations of the inhibitor

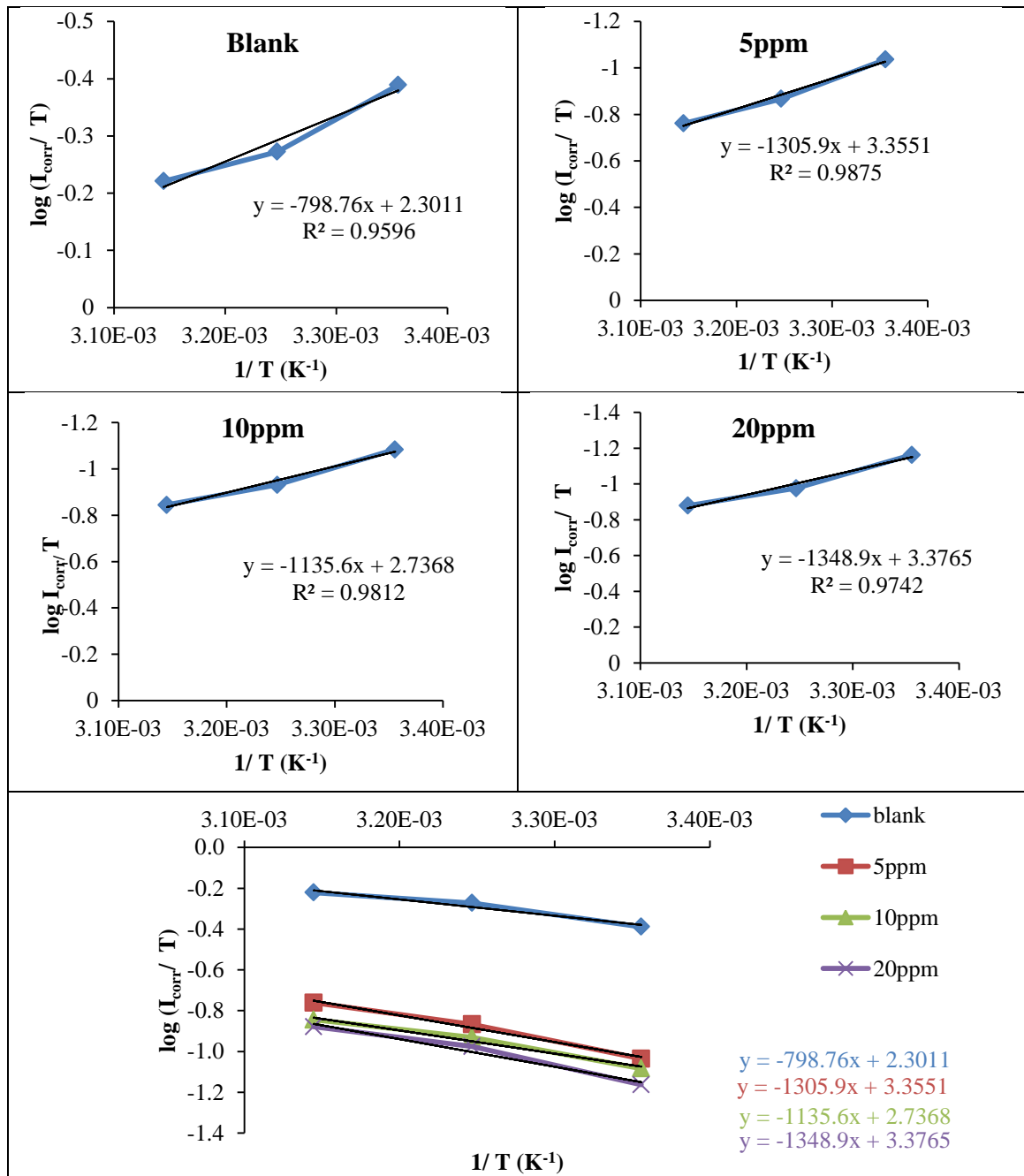


Figure 5-Plot for $\log(I_{corr}/T)$ vs $(1/T)$ of carbon steel in sea water for blank and in presence different concentrations of the inhibitor

Adsorption isotherm

The adsorption isotherms are useful to describe the reaction between the inhibitor molecules with carbon steel surface.

Langmuir adsorption isotherm can be represented by the following equation [19].

$$C/\theta = (1/K_{ads}) + C \tag{14}$$

Whereas C is the inhibitor concentration, K_{ads} is the adsorption/ desorption equilibrium constant. A plot of C/θ versus C, could be used to determine the equilibrium adsorption constant K_{ads} , then the thermodynamic functions, Figure-6. For the adsorption process, these functions are (ΔH_{ads} , ΔS_{ads} and ΔG_{ads}) represent in Table -11. ΔG_{ads} was calculated using Equation 15 [20].

$$\Delta G_{ads} = -2.303 RT \text{Log}(55.55K_{ads}) \tag{15}$$

Whereas R is the gas constant ($\text{J K}^{-1} \text{mol}^{-1}$), T is the absolute temperature (K), and 55.5 is the molar concentration (mol L^{-1}) of water in the solution. By plotting K_{ads} versus ($1/T$) the $\Delta G^{\circ}_{\text{ads}}$ was extracted from the slope entropy and enthalpy adsorption values by using Equations 15, 16, Figure-7.

$$\Delta G^{\circ}_{\text{ads}} = -RT \ln K_{\text{ads}} \quad (16)$$

$$\Delta G^{\circ}_{\text{ads}} = \Delta H^{\circ}_{\text{ads}} - T\Delta S^{\circ}_{\text{ads}} \quad (17)$$

Negative values of the $\Delta G^{\circ}_{\text{ads}}$ reflect the spontaneous adsorption. In general, values of $\Delta G^{\circ}_{\text{ads}}$ around or below (-40 kJ mol^{-1}) are compatible with physisorption and those around or more negative than (-40 kJ mol^{-1}) involve chemisorptions [21]. The calculated values for $\Delta G^{\circ}_{\text{ads}}$ have been found in the range of (-11.815 to $-12.672 \text{ kJ mol}^{-1}$) at different temperatures (298-318 K). These values fall between the threshold values for the physisorption.

The entropy $\Delta S^{\circ}_{\text{ads}}$ value was positive confirming that the corrosion process is entropically favorable [22]. The negative value of $\Delta H^{\circ}_{\text{ads}}$ indicate the adsorption of inhibitory molecules on the C.S surface is an exothermic process. For compound (3) $\Delta H^{\circ}_{\text{ads}}$ is equal to ($-13.717 \text{ kJ mol}^{-1}$) [23].

Table 11-Thermodynamic parameters for adsorption of compound (3) on C.S surface in 3.5% NaCl at various temperatures

T/ K	K_{ads}	ΔG kJ mol^{-1}	R^2	ΔH_{ads} kJ mol^{-1}	ΔS_{ads} $\text{kJ mol}^{-1} \text{K}^{-1}$
298	2.994012	-12.672	0.999	-13.717	0.0038
308	2.247191	-11.961	1.000		
318	2.118644	-11.815	0.999		

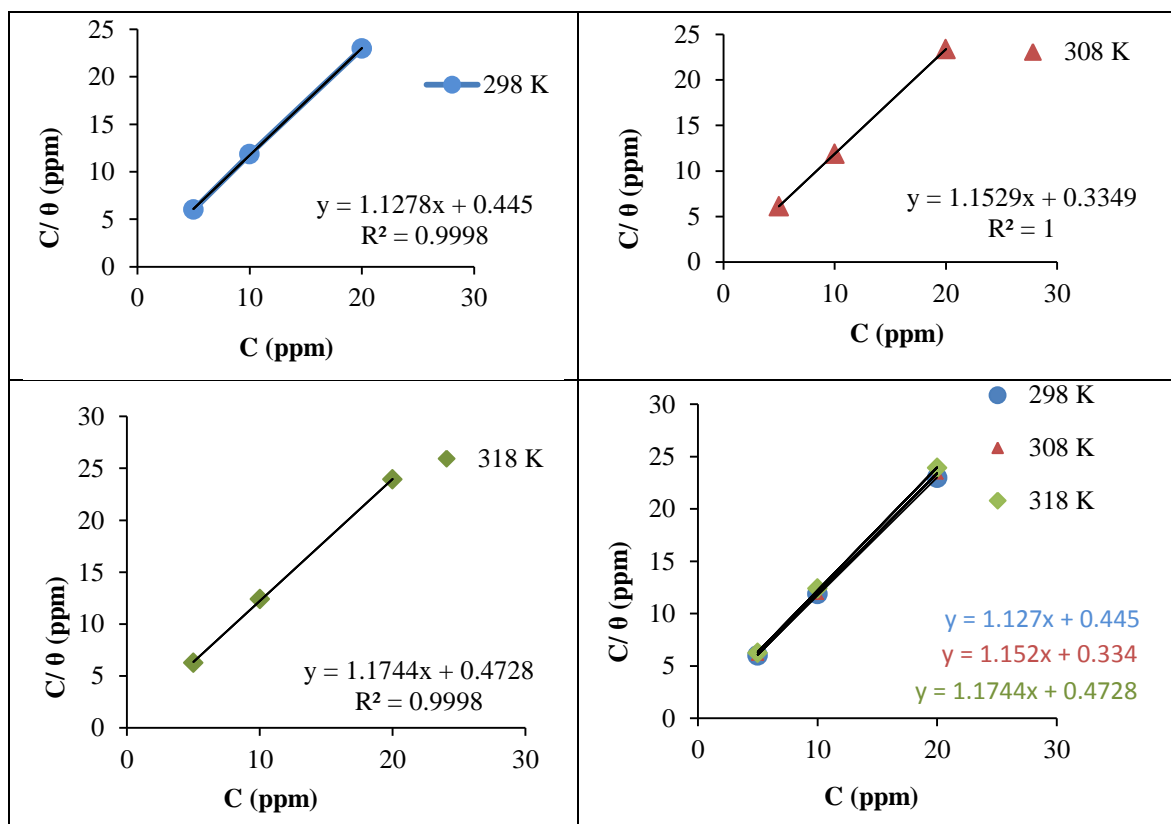


Figure 6-Langmuir isotherms plot for the adsorption compound (3) on carbon steel at the temperature range of (298, 308 and 318) K

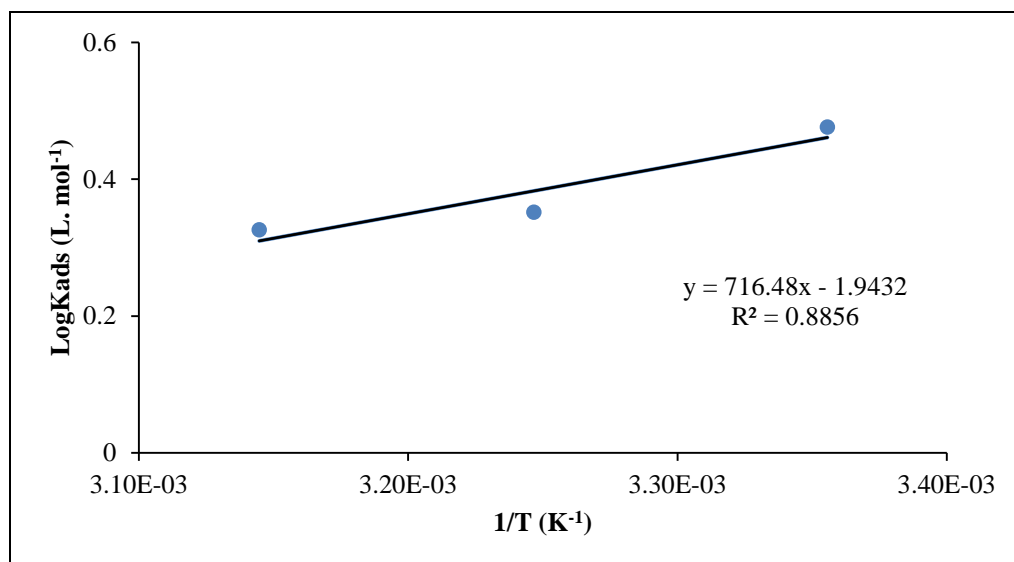


Figure 7-Plot of $\log K_{\text{ads}}$ vs $(1/T)$ for compound **(3)**

Scanning Electron Microscopy (SEM)

In Figure-8a, the badly damaged surface obtained when the metal was remained immersed in saline water. However, Figure-8b shown C.S surface in the presence of inhibitor **(3)** has respected smoothness as compared to Figure-8a, indicating reduction of the corrosion rate. This improvement in surface morphology is due to the formation of a protective film of compound **(3)** inhibitor on the C.S surface which is represent for inhibition of corrosion [24].

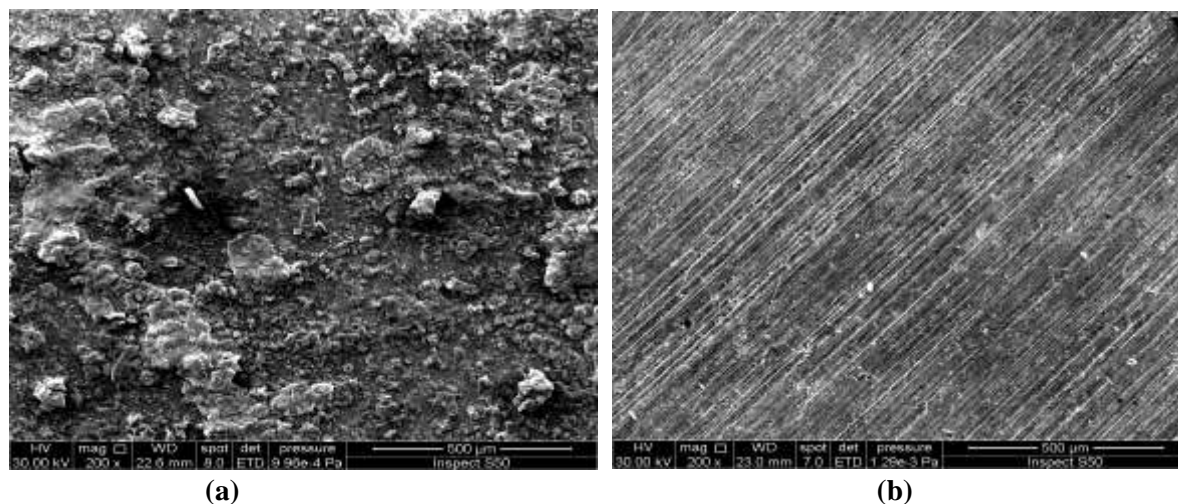


Figure 8-SEM images of carbon steel in a 3.5% NaCl solution at 318 K (a) without compound **(3)** inhibitor (b) in presence of compound **(3)** inhibitor.

Atomic force microscopy

Surface morphology of carbon steel sample in a 3.5% NaCl solution in the absence and presence of inhibitor **(3)** was investigated by atomic force microscopy (AFM). The results are shown in Figure-9 (a–f). The average roughness is clearly shown in Figure-9 (a, b and c) that carbon steel sample is badly damaged due to the 3.5% NaCl salt attack on the surface, The average roughness value (S_a), root mean square value; S_m (mean roughness value (S_q), peak valley height (S_y) for the carbon steel surface 2.79 nm, 4.11 nm, and 42.8 nm, respectively. However, in the presence of an optimum concentration (20 ppm) of compound **(3)** as shown in Figure-9 (d, e and f) the average roughness was reduced that display the steel surface after immersion in 3.5% NaCl presence of inhibitor. The (S_a), (S_q), (S_y) for the carbon steel surface are 19.4 nm, 25.7 nm and 257 nm, respectively [25].

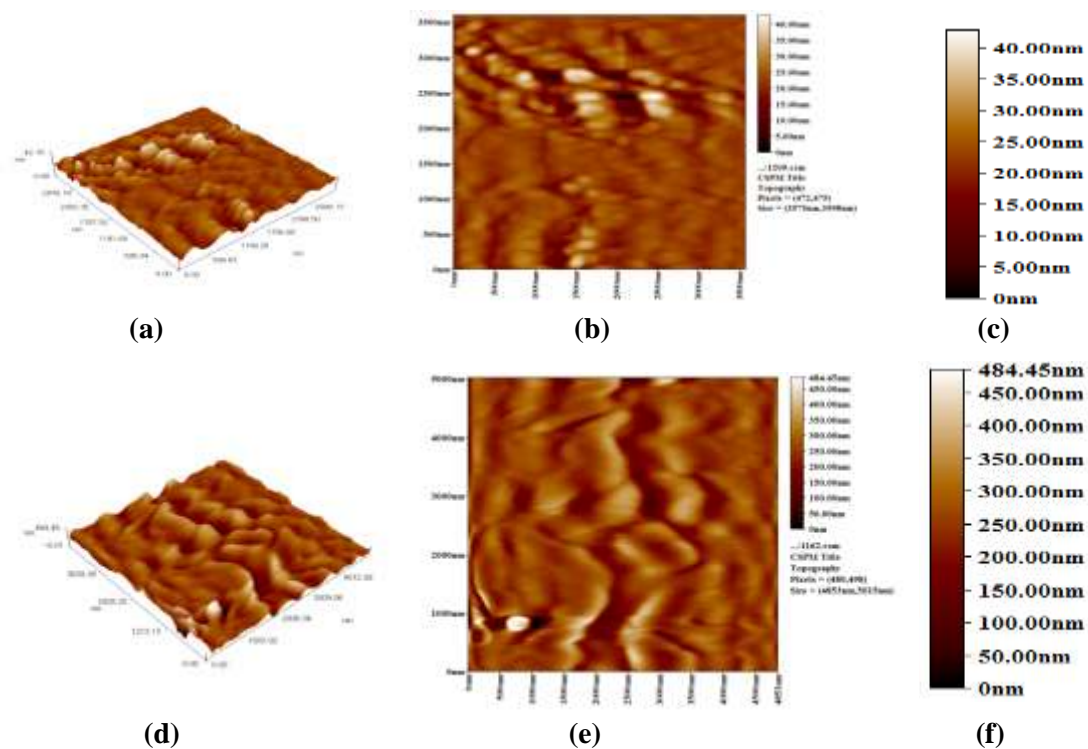


Figure 9-AFM of C.S surface (a, b, c) in a 3,5% NaCl solution, (d, e, f) in presence of 20 ppm compound (3).

Conclusion

1. The new synthesized isatin diazine derivatives (2-6), were theoretically found to be good organic corrosion inhibitors for carbon steel. The best one was compound (3).
2. The inhibition efficiency obtained for compound (3) experimentally using potentiodynamic polarization measurements, reflected that the studied inhibitor could be classified as a mixed inhibitor in 3.5% NaCl.
3. The inhibition efficiency increased with increasing inhibitor concentration.
4. The adsorptions of the studied compound on C-steel follow the Langmuir adsorption isotherm model. The low K_{ads} values indicate a physical reaction between the inhibitor and the metal surface, and the (ΔG°_{ads}) values suggested that the inhibition process may occur by physical adsorption process.

References

1. Zhenzhen, X. Guangcheng, W. Jing, W. Ming, C. Yaping, P. Luyao, L. Bing, D. Shan, C. and Wenbiao, L. **2017**. Synthesis, biological evaluation, and molecular docking studies of novel isatin-thiazole derivatives as α -glucosidase inhibitors. *Molecules*, **22** (659): 1-11.
2. Mohammad, A. **2017**. Various chemical and biological activities of pyridazinone derivatives, *Central European Journal of Experimental Biology*, **5**(1): 1-19.
3. El Bakri, Y. Boudalia, M. Echihi, S. Harmaoui, A. Sebhaoui, J. Elmsellem, H. Ramli, Y. Guenbour, A. Bellaouchou, A. and Essassi, E. **2017**. Performance and theoretical study on corrosion inhibition of new Triazolopyrimidine derivative for Carbon steel in hydrochloric acid. *Journal of materials and Environmental Sciences*, **8** (2): 378-388.
4. David, A. **2017**. Predicting the performance of organic corrosion inhibitors. *Metals*, **7** (553): 1-8.
5. Aouniti, A. Elmsellema, H. Tighadouini, S. Elazzouzi, M. Radi, S. Chetouani, A. Hammouti, B. and Zarrouk, A. **2016**. Schiff's base derived from 2-acetyl thiophene as corrosion inhibitor of steel in acidic medium. *Journal of Taibah University for Science*, **10**: 774-785.

6. Suaad, M. and Redhab, A. **2015**. Synthesis and evaluation antimicrobial activity of some new S-substituted quinazolinone containing pentagonal, hexagonal heterocyclic ring. *Journal of Zankoi Sulaimani*, **17**(1): 33-48.
7. Athraa, H. Suaad, M. and Rehab, M.K. **2018**. Synthesis, identification, theoretical and experimental studies for carbon steel corrosion inhibition in sea water by some new schiff base derivatives linkage to 5-nitro isatin moiety, *Journal of Global Pharma Technology*, JGPT V(10) No. (9-10) September-October, Accepted for publishing.
8. Frolov, E. Lakner, F. and Khvat, A. **2004**. An efficient synthesis of novel 1, 3- oxazolo [4,5-d]pyridazinones. *Tetrahedron Letter*, **45**: 4693-4696.
9. Rajendran, M. Keerthika, K. Kowsalya, M. and Devapiriam, D. **2016**. Theoretical studies on corrosion inhibition efficiency of pyridine carbonyl derivatives using DFT method. *Der Pharma Chemica*, **8** (3): 71-79.
10. Frisch, M. Trucks, W. Schlegel, G. Scuseria, H. Robb, G. Cheeseman, M. Montgomery, J. Vreven, J. Kudin, T. Burant, K. Millam, J. Iyengar, J. Tomasi, S. Barone, J. Mennucci, V. Cossi, B. Scalmani, M. Rega, G. Petersson, N. Nakatsuji, G. Hada, H. Ehara, M. Toyota, M. Fukuda, K. Hasegawa, R. Ishida, J. Nakajima, M. Honda, T. Kitao, Y. Nakai, O. Klene, H. Li, M. Knox, X. Hratchian, J. Cross, H. Bakken, J. Adamo, V. Jaramillo, C. Gomperts, J. Stratmann, R. Yazyev, R. Austin, O. Cammi, A. Pomelli, R. Ochterski, C. Ayala, J. Morokuma, P. Voth, K. Salvador, G. Dannenberg, P. Zakrzewski, J. Dapprich, V. Daniels, S. Strain, A. Farkas, M. Malick, O. Rabuck, D. Raghavachari, A. Foresman, K. Ortiz, J. Cui, J. Baboul, Q. Clifford, A. Cioslowski, S. Stefanov, J. Liu, B. Liashenko, G. Piskorz, A. Komaromi, P. Martin, I. Fox, R. Keith, D. Al-Laham, T. Peng, M. Nanayakkara, C. Challacombe, A. Gill, M. Johnson, P. Chen, B. Wong, W. Gonzalez, M. and Pople, J. Gaussian 03, Gaussian. Inc. Pittsburgh PA, **2009**.
11. Becke, A. **1993**. Density-functional thermochemistry. III. The role of exact exchange. *Journal of Chemistry and Physical*, **98**: 5648-5652.
12. Ee, C. Yang, W. and Parr, R. **1988**. Development of the colle-salvetti correlation-energyformula into a functional of the electron density. *Physical Review*, **B 41**: 785-789.
13. Rehab, M. and Mustafa, M. **2016**. Theoretical studies of corrosion inhibition efficiency of two new N-phenyl-ethylidene-5-bromo isatin derivatives. *Iraqi Journal of Science*, **57** (2B): 1041-1051.
14. Raafat, M. Mohamed, K. and Faten, M. **2008**. Quantum chemical studies on the inhibition of corrosion of copper surface by substituted uracils. *Applied Surface Science*, **255**: 2433-2441.
15. Henriquez-Román, J. Sancy, M. Páez, M. Padilla-Campos, L. Zagal, J. Rangel, C. and Thompson, G. **2005**. The influence of aniline and its derivatives on the corrosion behaviour of copper in acid solution. *Journal of Solid State Electrochemistry*, **9** (7): 504-511.
16. Rehab, M. and Fatten, K. **2015**. DFT, PM3, AM1, and MINDO/3 quantum mechanical calculations for some INHC Cs symmetry schiff bases as corrosion inhibitors for mild steel. *Iraqi Journal of Science*, **56**(1C): 602-621.
17. Ben Hmamou, D. Aouad, M. Salghi, R. Zarrouk, A. Assouag, M. Benali, O. Messali, M. Zarrok, H. and Hammouti, B. **2012**. Inhibition of C38 steel corrosion in hydrochloric acid solution by 4,5-diphenyl-1H-imidazole-2-thiol:gravimetric and temperature effects treatments. *International Journal of Science and Research*, **4** (7): 3498- 3504
18. Abd-El-Naby, B. Abdullatef, O. Khamis, E. and El-Mahmody, W. **2016**. Effect of cetyltrimethylammonium bromide surfactant as novel inhibitor for the corrosion of steel in 0.5 M H₂SO₄. *International Journal Electrochemistry and Science*, **11**: 1271-1281.
19. Uday, H. Suaad, M. and Khulood, A. **2013**. Corrosion inhibition effects of some new synthesized N-Aroyl-N\Aryl thiourea derivatives for carbon steel in sulfuric acid media. *Journal of Al-Nahrain University*, **16** (4): 80-93.
20. Rehab, M. Dhuha, A. and Suaad, M. **2017**. Quantum mechanical and electrochemical study of new isatin derivative as corrosion inhibitor for carbon steel in 3.5 % NaCl. *International Journal of Science and Research*, **6** (7): 1656-1669.
21. Hong, S. Chen, W. Luo, H. and Li, N. **2012**. Inhibition effect of 4-amino-antipyrine on the corrosion of copper in 3 wt. % NaCl solution. *Corrosion Science*, **57**: 270-278.

22. Issa, R. El-Sonbati, A. El-Bindary, A. and Kera, H. **2002**. Potentiometric and thermodynamic studies of 2-acrylamidosulfamethazine and its metalcomplexes. *Journal of Eurpan Polymar*, **38**: 561.
23. El-Ouali, I. Hammouti, B. Aouniti, A. Ramli, Y. Azougagh, M. Essassi, E. and Bouachrine, M. **2010**. Thermodynamic Characterisation of Steel Corrosion in HCl in the Presence of 2-Phenylthieno (3, 2-b) Quinoxaline. *Journal of Material and Enviromantal Science*, **1** (1): 1-8.
24. Mohamed, A. Khaled, Z. Hamdy, A. Abo-Elenien, O. and Olfat, E. **2015**. Synthesis of novel schiff base silicon compound for employing as corrosion inhibitor for carbon steel in the 1 M HCL and 3.5% NaCl aqueous media. *International Journal of Chemical, Environmental & Biological Sciences*, **3**: 2320-4087
25. Gowri, S. Sathiyabama, J. Prabhakar, P. and Rajendran, S. **2012**. Inhibition behaviour of carbon steel in sea water in the presence of tyrosine- Zn^{2+} system. *International Journal of Research in Chemistry and Environment*, **3**: 156-162.